Dalton Transactions

ROYAL SOCIETY OF CHEMISTRY

COMMUNICATION

View Article Online
View Journal

Cite this: DOI: 10.1039/d0dt02190c

Received 20th June 2020,
Accepted 20th July 2020

DOI: 10.1039/d0dt02190c

rsc.li/dalton

Solution aggregation of platinum(II) triimine methyl complexes†

Vikas M. Shingade * and William B. Connick‡

The NMR chemical shifts of [Pt(tpy)(CH$_3$)](PF$_6$) (1) and [Pt(mbzimpy)(CH$_3$)](PF$_6$) (2), where tpy = 2,2′;6′2″-terpyridine and mbzimpy = 2,6-bis(*N*-methylbenzimidazol-2-yl)pyridine, in room-temperature DMSO-d_6 displayed concentration dependence as a result of formation of dimers. Quantification of these dimers, expressed by equilibrium constant (*K*), shows a greater tendency of 2 to aggregate in solution. Structural conformations of these dimers were confirmed by 2D ^{1}H–^{1}H NOESY; the results explicitly suggest a head-to-tail stacking arrangement of molecules in dimers.

A well-known property of late 2nd and 3rd row d^8-electron transition metal complexes is their tendency to self-assemble in solutions, which can have dramatic consequences for the colors and other spectroscopic properties of these systems.[1–8] In the case of platinum(II) complexes with triimine chelates, such as Pt(tpy)Cl$^+$, the consensus view is that aggregation is driven mainly by Pt···Pt and ligand π···π interactions.[1–5,9] Several literature reports on terpyridine-based platinum(II) complexes demonstrate the use of electronic absorption and ^{1}H NMR spectroscopies to gain insight into the nature of aggregates.[1,10–16] The work of Romeo *et al.* using the aforementioned spectroscopies demonstrated that Pt(tpy)(CH$_3$)$^+$ forms dimers in dilute aqueous solution and larger aggregates when the concentration and/or ionic strength increases.[10,12,14,15] Despite the fact that Pt(tpy)(CH$_3$)$^+$ and many other platinum(II) compounds have been extensively investigated for their intriguing spectroscopic and photophysical properties,[1,3,4,9,17–20] solution structures of these self-assemblies, which strongly influence these properties, have remained elusive. Knowledge of these structures is important to efforts aimed at exploiting the self-assembly for applications such as chemosensing, supramolecular chemistry, host–guest chemistry, and biomolecular interactions.[19,21] Our interest in the class of platinum(II) triimine complexes stems from our discovery of luminescent Pt(mbzimpy)Cl$^+$ salts and related compounds that display interesting chemosensing properties as a result of interactions noted above.[22–26] In principle, solid-state structures may give some insight into the nature of stacking interactions. However, given the relatively weak forces involved, it is not obvious that aggregates formed in solution will necessarily retain their preferred conformation when precipitated. A warning of the potential pitfalls of such assumptions was highlighted in a recent study of the vapochromism of yellow [Pt(tpy)Cl](ClO$_4$), which turns red upon exposure to water vapor.[27] Loss of water vapor restores the original yellow color, but this yellow material has a different packing arrangement than crystals of [Pt(tpy)Cl](ClO$_4$) precipitated from solution. To better understand the preferred stacking conformation in such complexes, herein, we have investigated the aggregation of two model complexes in Scheme 1 in DMSO-d_6 by means of NMR and UV-vis absorption spectroscopy.

The hexafluorophosphate salt of the terpyridyl complex **1** was prepared from the reaction of PtClMe(SMe$_2$)$_2$ with terpyridine followed by anion methathesis, as previously described.[28,29] **2** was prepared in an analogous fashion. The complexes were fully characterized, including assignment of the ^{1}H NMR chemical shifts using a combination of 2D COSY

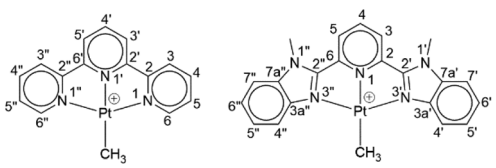

1 **2**

Scheme 1 Molecular structures and atom numbering for complexes **1** and **2**. (PF$_6$)$^-$ is the counterion.

Department of Chemistry, University of Cincinnati, P.O. Box 210172, Cincinnati, OH 45221-0172, USA. E-mail: vikas.shingade@gmail.com

†Electronic supplementary information (ESI) available: Synthesis, characterization, NMR and absorption spectra, table of absorption maxima, equations and calculations, and relevant plots and data fitting summaries. See DOI: 10.1039/d0dt02190c

‡Professor William B. Connick passed away in 2018.

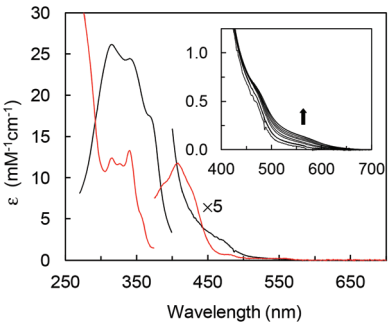

Fig. 1 Apparent molar absorptivities of 0.3 mM solutions of **1** (—) and **2** (—) in DMSO. Inset: visible absorption spectra of **2** over the 0.3–32 mM concentration range.

and NOESY experiments. Both complexes dissolve in DMSO to give pale yellow solutions at low concentrations. However, the solutions darken and become dark red as the solubility limits are approached (**1**, 0.25 M; **2**, 0.04 M). To better characterize this behavior, the electronic absorption spectra were recorded (Fig. 1 and Table S1 ESI†). The main features of the spectra of such complexes have previously been discussed.[1,10,22,30,31] Notably, characteristic vibronic structure of the triimine-centered $^1(\pi \rightarrow \pi^*)$ transitions ($\varepsilon \approx 10^4$ M^{-1} cm^{-1}) occurs in the 300–370 nm range for **1** and 280–390 nm range for **2**. A ^{1}MLCT [d(Pt) $\rightarrow$ π^*(triimine)] band ($\varepsilon \approx 10^3$ M^{-1} cm^{-1}) occurs at longer wavelengths, near 408 nm in the spectrum of **1** and at 468 nm in the spectrum of **2**. With increasing concentration, new features appear in the long wavelength region (450–600 nm) of the spectra of **1** and **2** (Fig. 1 (inset), Fig. S6, ESI†), which display broadening and increasing molar extinction coefficients. The non-Beer's law behavior (or the hyperchromicity) of these features is indicative of formation of aggregates. Furthermore, the origin of these features is consistent with the ^{1}MMLCT transitions.[1,13]

Concentration dependence of the chemical shifts

Each of the ^{1}H NMR chemical resonances of **1** and **2** in DMSO-d_6 are concentration dependent (Fig. S1–S4 ESI†), shifting monotonically upfield and broadening with increasing concentration. These observations are consistent with a dynamic equilibrium between the monomer and an aggregate with a stacked geometry. It should be noted that the ^{1}H NMR chemical shifts of the free ligands, tpy and mbzimpy, are invariant over these concentration ranges, indicating that the free ligands do not aggregate under these conditions. The total shift ($\Delta\delta_c$) for a given a proton over the investigated concentration (c) range (**1**, 0.09–240 mM; **2**, 0.09–35 mM) gives an indication of the resonance's sensitivity to concentration (Scheme S1 ESI†). Interestingly, protons of **1** and **2** show a wide range of $\Delta\delta_c$ values, which is consistent with the notion that the deshielding is dependent on the specific stacking geometry of an aggregate. Also, at equivalent concentration range, for example at 0.09–35 mM, the $\Delta\delta_{35}$ value for a given a proton of **1**, excepting for $H_{4'}$, is relatively lower than that for a similar proton of **2**. Besides, the $\Delta\delta_c$ values for Pt-methyl protons are relatively higher than the $\Delta\delta_c$ values for rest of the protons due to the stronger shielding resulted of the ring current. This suggests its location near one of the rings of triimine ligand. Further, it stands to reason that a head-to-head conformation may not be the preferred way of stacking interaction in these molecules.

Interestingly, at the lowest concentrations ($\lesssim$10 mM), the ^{1}H NMR spectrum of **2** exhibited additional resonances that display growing dominance with the lowering of concentration (Fig. S2, ESI†). The identity of these resonances is consistent with that of the free mbzimpy ligand, which indicates a complete dissociation of mbzimpy from **2**. The ligand dissociation constant was estimated to be in the range of 3×10^{-6} to 3×10^{-5} M, and it suggest that a stacking structure provides stability to **2** from undergoing ligand dissociation in DMSO solution. Down to 0.09 mM, the spectra of **1** showed no evidence of free tpy ligand, suggesting that the dissocation constant for tpy is at least 3×10^3 times lesser than that for mbzimpy; a contributing factor to this enhanced stability may be the more optimal bite angle favored by the 6-membered pyridyl rings of tpy, as compared to the 5-membered rings of mbzimpy.

Because the methyl protons were the most sensitive to the concentration, methyl proton chemical shifts of **1** and **2** (Fig. 2) were fitted to a model describing the dynamic equilibrium between a monomer (M) and an aggregate (M_n):

$$nM \rightleftharpoons M_n \quad (1)$$

Fits to models involving a higher order aggregate (M_n, $n > 2$) were inferior. The data were sufficiently well described ($R^2 > 0.999$) that fits models involving more than one aggregate were not justified.

For **2**, the resulting dimerization constant (K) obtained based on the N-CH_3 chemical shift was in excellent agreement with that obtained from the variation in the Pt-CH_3 chemical shift (Fig. 2, Fig. S5; Tables S3 and S4, ESI†). Interestingly, K for **2** is about ten times higher than that for **1** (Tables 1; and S2–S4, ESI†), which suggests a greater tendency of **2** to aggregate in solution. This conclusion also is consistent with the relative solubilities of complexes, as well as the $\Delta\delta_c$ values over similar concentration ranges (Scheme S1, ESI†).

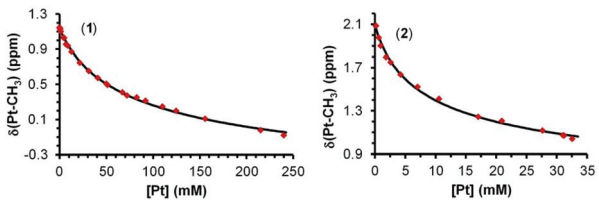

Fig. 2 Pt-Methyl proton chemical shifts for **1** and **2** *vs.* concentration. Solid black line shows best fit to a monomer–dimer dynamic equilibrium model (R^2 = 0.9998).

Table 1 Dimerization constants determined from ^{1}H NMR chemical shift[a] and 560 nm electronic absorption[b] data in DMSO-d_6

Complex	^{1}H Resonance	K^a (M^{-1})	K^b (M^{-1})	ε^b (M^{-1} cm^{-1})
1	δ(Pt-CH_3)	6.2 ± 0.8	17 ± 2	354 ± 2
2	δ(Pt-CH_3)	59 ± 16	72 ± 4	476 ± 1
2	δ(N-CH_3)	61 ± 16	—	—

[a] 95% linear confidence intervals. Upper and lower bounds on lack-of-fit confidence region are provided in ESI.† [b] Fitting of electronic absorption data is provided in ESI.†

Fitting of the electronic absorption data using the same model (eqn (1)),[1,11] yielded comparable dimerization constants (K), 17 ± 2 M^{-1} for **1** and 72 ± 4 M^{-1} for **2** (Table S5, Fig. S6 ESI†). This analysis also yields estimates for the molar absorptivities of the dimer (**1**, 354 ± 2 M^{-1} cm^{-1}; **2**, 476 ± 1 M^{-1} cm^{-1}), which are decidedly less than values observed for the ^{1}MMLCT band of authentic Pt(tpy) dimers (2000–4000 M^{-1} cm^{-1}),[2,32,33] which consist of two covalently bridged Pt(tpy) units resulting in a dimer with approximate C_{2v} symmetry. Faced with a similar discrepancy in the case of Pt(tpy)Cl^+ dimerization in 0.1 M aqueous NaCl, Bailey *et al.* suggested the possibility that a second dimer also forms in solution, namely one supported by tpy π–π interactions but lacking the Pt···Pt interactions necessary to give intensity to a ^{1}MMLCT band.[1] Making a similar assumption of ε(MMLCT) = 2000 M^{-1} cm^{-1} for the metal–metal (MM) dimer and applying this treatment to our data (Table S6 ESI†), we obtained estimates of the dimerization constants for the ligand–ligand (ππ), and metal–metal (MM) supported dimers ($K_{\pi\pi}$ and K_{MM}: **1**, 13.7 M^{-1} and 3.0 M^{-1}; **2** 54.7 M^{-1} and 17.1 M^{-1}). However, it should be emphasized that both the NMR and UV-visible data are adequately modeled according to a single dimer model (eqn (1)), and the justification for the two dimer model rests entirely on expectations concerning the molar absorptivity. Therefore, another possible explanation for the comparatively low molar absorptivities derived from the single-dimer model is that the oscillator strength of the MMLCT band of C_{2h}-symmetric head-to-tail dimers is intrinsically weaker.

Comparison of the dimerization constants for **1** and **2** with those previously determined[15] K values for **1** and related compounds were expected to provide insights into the factors influencing dimerization. For example, K for **1** of 26(1) × 10^3 M^{-1} in D_2O by ^{1}H NMR and 10(8) × 10^3 M^{-1} in a buffer (1 mM Phosphate + 0.1 M $NaCl_{(aq)}$, pH = 7.0) by UV-vis absorption techniques reveals a large difference between K values. This difference is consistent with a notion that a lower dielectric constant of DMSO disfavors formation of dicationic dimer whereas intermolecular hydrophobic interactions favor stacking in water. On the other hand, a survey of K values[1,11,13] of Pt(tpy)Cl^+, 4(2) × 10^3 M^{-1} in water and 3(2) × 10^3 M^{-1} in 0.1 M $NaCl_{aq}$, suggests that a substitution of chloro- ligand by methyl- group increases a tendency of Pt-tpy complex to aggregate in solution. This observation is in accord with the smaller size of the chloro group and the stronger σ-donor properties of a methyl group, which are expected to enhance metal···metal interaction.[34]

Molecular structure of a dimer

The 2D ^{1}H–^{1}H NOESY was employed to elucidate structural conformations of a dimer of **1** and **2** in DMSO-d_6. In order to estimate distance restraints for weak NOEs,§ the NOESY experiments also were performed on free ligands. The free ligand NOE spectra (Fig. S7 and S9 ESI†) exhibit no signs of NOEs between protons separated by ≥4.6 Å. The spectra also suggest that free ligands have non-planar geometries in solutions.

For the structural analysis of **1** and **2** dimers, the focus was given in particular to the long-range (weak) NOEs. The discrimination between intra- and intermolecular NOEs was based upon the distance restraint of 5.0 Å above which any sign of NOE was assessed for intermolecular interaction. Furthermore, the absence of some key NOE cross-peaks offered undoubted assignments of some long-range NOEs to inter- rather than intramolecular protons. For example, the NOE spectrum of **1** (Fig. S8 ESI†) exhibits no sign of NOE between Pt-C$\mathbf{H_3}$···$\mathbf{H}_{(4,\ 4'')}$ protons separated by distance (d) of ~6.0 Å in monomer, however, medium NOE cross-peak was observed between Pt-C$\mathbf{H_3}$···$\mathbf{H}_{(3',\ 4',\ 5')}$ (d, ≥7.0 Å), which suggests intermolecular interactions between these protons. Similarly, a weak NOE cross-peak was observed between Pt-C$\mathbf{H_3}$···$\mathbf{H}_{(3,\ 3'')}$ (d, ~6.2 Å). These results strongly indicate a head-to-tail fashioned interaction in a dimer of **1**.

In the case of **2**, fewer NOE contacts helped to illustrate the structure more clearly (Fig. 3). Similar to the **1**, no signs of NOEs were observed between Pt-C$\mathbf{H_3}$···$\mathbf{H}_{(6',\ 6'',\ 7',\ 7'')}$ (d, >5.8 Å), $\mathbf{H}_{(7',\ 7'')}$···$\mathbf{H_4}$ (d, ~7.7 Å) and $\mathbf{H}_{(6'/6'')}$···$\mathbf{H}_{(3/5,\ 4)}$ (d, >7.5 Å). Whereas, weak NOEs were observed between protons Pt-

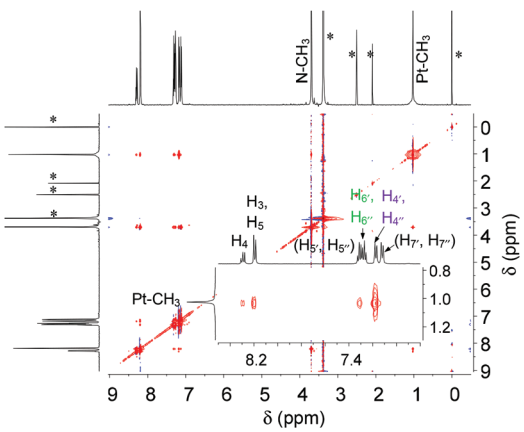

Fig. 3 2D ^{1}H–^{1}H NOESY spectrum of 35 mM DMSO-d_6 solution of **2**. Inset: partial 2D NOESY of **2**.

$CH_3\cdots H_{(3/5,\ 4)}$ (d, ≥7.0 Å), Pt-$CH_3\cdots$N-CH_3 (d, ≥7.0 Å), and N-$CH_3\cdots H_{(4',\ 4'',\ 5',\ 5'')}$ (d, ~6.0 Å). These NOEs strongly indicate head-to-tail fashioned interactions of molecules in a dimer of **2** as well.

The NOE data of **2** was further analyzed by applying a dimer model in various stacking arrangement of molecules. For this analysis, we used 5 Å as the upper bound of distance restraints for any sign of NOE contacts. The modeling results indicate that all NOE constraints of **2** are well satisfied in an anti-parallel displaced conformation of a dimer with molecules rocking along *x*- and *y*-directions in a symmetrical fashion within a molecular plane. Moreover, the model shows dominance of ligand···ligand interactions with no appreciable Pt···Pt contact. On the other hand, as expected, a model with face-to-face interactions violates NOE constraints. Thus, our NOE based structural model implicitly supports the formation of **2** dimer in a head-to-tail geometry.

Similar to **2**, the NOE data of **1** are consistent with an anti-parallel arrangement of molecules in a dimer. However, the detection of fewer intermolecular NOE contacts limits our efforts to show that ligand···ligand interactions dominate in a dimer of **1** as well. Fitting results of 560 nm absorptions (*vide supra*), however, are more conclusive in this regard. From the spectroscopy and fitting results discussed above, it is apparent that the aggregation is relatively stronger in **2**, and the structure of a dimer is controlled by multiple types of interactions,[35] mainly ligand···ligand and Pt···Pt interactions. To further support this assessment we note that the ^{13}C chemical shift for the Pt-CH_3 group of **2** was observed relatively upfield due to the ring current (δ, −25.6 ppm for **2** at 29.4 mM and −5.14 ppm for **1** at 240 mM) at nearly equivalent dimer : monomer ratios of the complexes in dmso-d_6. On the other hand, metal···metal interaction is noticeably weak in **1** and **2** dimers. All these results suggest that the ligand···ligand interaction majorly drives aggregation in our complexes, and it shapes a structural geometry of a dimer.

In summary, the 2D NOE spectra of **1** and **2** provide the first definitive evidence of a head-to-tail dimer formation in fluid solution. Further, fittings of the NOE and the electronic absorption data support the notion that the forces that are stabilizing these dimers are dominated by ligand···ligand interactions in lower dielectric solvents. In the case of **2**, the intermolecular interactions stabilizing the dimer are decidedly stronger. Also, a dimeric structure gives chemical stability to **2** from undergoing decomposition.

Conflicts of interest

There are no conflicts to declare.

Acknowledgements

We thank Dr Keyang Ding (NMR facility manager at the University of Cincinnati) for expert technical assistance with NMR. This work was supported by the National Science Foundation (NSF Grants CHE-1152853 and CHE-1566438).

Notes and references

§ NOE strength (distance restraint): strong (<2.5 Å), medium (<3.7 Å), weak (<5 Å).

1 J. A. Bailey, M. G. Hill, R. E. Marsh, V. M. Miskowski, W. P. Schaefer and H. B. Gray, *Inorg. Chem.*, 1995, **34**, 4591–4599.
2 J. A. Bailey, V. M. Miskowski and H. B. Gray, *Inorg. Chem.*, 1993, **32**, 369–370.
3 V. M. Miskowski and V. H. Houlding, *Inorg. Chem.*, 1989, **28**, 1529–1533.
4 V. M. Miskowski, V. H. Houlding, C. M. Che and Y. Wang, *Inorg. Chem.*, 1993, **32**, 2518–2524.
5 V. H. Houlding and V. M. Miskowski, *Coord. Chem. Rev.*, 1991, **111**, 145–152.
6 I. S. Sigal and H. B. Gray, *J. Am. Chem. Soc.*, 1981, **103**, 2220–2225.
7 K. R. Mann, J. G. Gordon II and H. B. Gray, *J. Am. Chem. Soc.*, 1975, **97**, 3553–3555.
8 V. W.-W. Yam, K. M.-C. Wong and N. Zhu, *J. Am. Chem. Soc.*, 2002, **124**, 6506–6507.
9 K. M.-C. Wong and V. W.-W. Yam, *Acc. Chem. Res.*, 2011, **44**, 424–434.
10 G. Arena, G. Calogero, S. Campagna, L. M. Scolaro, V. Ricevuto and R. Romeo, *Inorg. Chem.*, 1998, **37**, 2763–2769.
11 K. W. Jennette, J. T. Gill, J. A. Sadownick and S. J. Lippard, *J. Am. Chem. Soc.*, 1976, **98**, 6159–6168.
12 R. Romeo, L. M. Scolaro, M. R. Plutino and A. Albinati, *J. Organomet. Chem.*, 2000, **593–594**, 403–408.
13 M. G. Hill, J. A. Bailey, V. M. Miskowski and H. B. Gray, *Inorg. Chem.*, 1996, **35**, 4585–4590.
14 R. Romeo, G. Arena, L. Monsù Scolaro and R. F. Pasternack, *Nuovo Cimento Soc. Ital. Fis., D*, 1994, **16D**, 1523–1528.
15 G. Arena, L. M. Scolaro, R. F. Pasternack and R. Romeo, *Inorg. Chem.*, 1995, **34**, 2994–3002.
16 A. R. Petersen, R. A. Taylor, I. Vicente-Hernandez, J. Heinzer, A. J. P. White and G. J. P. Britovsek, *Organometallics*, 2014, **33**, 1453–1461.
17 A. Y.-Y. Tam, W. H. Lam, K. M.-C. Wong, N. Zhu and V. W.-W. Yam, *Chem. – Eur. J.*, 2008, **14**, 4562–4576.
18 D. R. McMillin and J. J. Moore, *Coord. Chem. Rev.*, 2002, **229**, 113–121.
19 I. Eryazici, C. N. Moorefield and G. R. Newkome, *Chem. Rev.*, 2008, **108**, 1834–1895.
20 K. M.-C. Wong, W.-S. Tang, B. W.-K. Chu, N. Zhu and V. W.-W. Yam, *Organometallics*, 2004, **23**, 3459–3465.
21 A. J. Goshe, I. M. Steele and B. Bosnich, *J. Am. Chem. Soc.*, 2003, **125**, 444–451.

22 L. J. Grove, J. M. Rennekamp, H. Jude and W. B. Connick, *J. Am. Chem. Soc.*, 2004, **126**, 1594–1595.
23 L. J. Grove, A. G. Oliver, J. A. Krause and W. B. Connick, *Inorg. Chem.*, 2008, **47**, 1408–1410.
24 E. J. Rivera, C. Barbosa, R. Torres, L. Grove, S. Taylor, W. B. Connick, A. Clearfield and J. L. Colon, *J. Mater. Chem.*, 2011, **21**, 15899–15902.
25 J. R. Kumpfer, S. D. Taylor, W. B. Connick and S. J. Rowan, *J. Mater. Chem.*, 2012, **22**, 14196–14204.
26 V. M. Shingade, Ph.D. Dissertation, University of Cincinnati, 2016.
27 S. D. Taylor, A. E. Norton, R. T. Hart, M. K. Abdolmaleki, J. A. Krause and W. B. Connick, *Chem. Commun.*, 2013, **49**, 9161–9163.
28 A. W. Addison, S. Burman, C. G. Wahlgren, O. A. Rajan, T. M. Rowe and E. Sinn, *J. Chem. Soc., Dalton Trans.*, 1987, 2621–2630.
29 G. S. Hill, M. J. Irwin, C. J. Levy, L. M. Rendina and R. J. Puddephatt, *Inorg. Synth.*, 1998, **32**, 149–153.
30 I. Mathew and W. Sun, *Dalton Trans.*, 2010, **39**, 5885–5898.
31 V. M. Shingade, L. J. Grove and W. B. Connick, *Dalton Trans.*, 2020, **49**, 9651–9661.
32 E. M. A. Ratilla, B. K. Scott, M. S. Moxness and N. M. Kostic, *Inorg. Chem.*, 1990, **29**, 918–926.
33 K. M.-C. Wong, N. Zhu and V. W.-W. Yam, *Chem. Commun.*, 2006, 3441–3443.
34 W. B. Connick, R. E. Marsh, W. P. Schaefer and H. B. Gray, *Inorg. Chem.*, 1997, **36**, 913–922.
35 C. Janiak, *J. Chem. Soc., Dalton Trans.*, 2000, 3885–3896.